

Investigation of Antenna Array Configurations Using Far-Field Holographic Microwave Imaging Technique

Lulu Wang^{1, *}, Ahmed M. Al-Jumaily¹, and Ray Simpkin²

Abstract—Biomedical imaging has played an important role in identifying and monitoring the effectiveness of the current state of the art treatments for many diseases. The authors recently proposed a novel single-transmitter-multiple-receiver holographic microwave imaging (HMI) technique for imaging small inclusion embedded in a dielectric object which has potential application in medical diagnostics. HMI image quality depends highly on the antenna baseline difference, in order words, the antenna array configuration. Different antenna arrays produce different quality of dielectric images by using HMI imaging algorithm. This paper investigates the antenna array configurations effect on image quality by using HMI imaging approach. Three configurations including spiral, random and regularly spaced arrays are presented. Both simulated and experimental results are obtained and compared to fully demonstrate the effectiveness of antenna arrays to the HMI technique. The results show that the proposed spiral and random array configurations have an ability to produce high-resolution images at significantly lower costs than regularly spaced arrays.

1. INTRODUCTION

Microwave imaging techniques have been proposed as one of the most promising complimentary techniques to X-ray mammography for early detection of breast cancer, which have attracted many groups of investigators [1–8] among engineers, clinicians, physiologists, pathologists and biochemists over the past two decades.

Creating high-resolution microwave breast images at lower costs has been studied by many [5–8], which includes antenna design, optimization of antenna array configuration (also named as array geometry) and investigation of image algorithms. The most common types of antenna arrays in microwave imaging for breast lesion detection are planar [5] and cylindrical [8] ones. Both of them are regularly spaced array configurations. The planar configuration uses a 2-D array of antennas placed on the naturally flat breast with the patient lying in the supine position. In data measurement, each antenna in the array sequentially illuminates the breast with an ultra-wideband pulse and that antenna alone records the backscatter. Conversely, the circular configuration involves the patient lying in the prone position with the breast surrounded by a circular array of antennas. In data collection, each antenna in the array once again sequentially illuminates the breast, but this time the back-scattered signals are recorded at all of the antenna array elements located at different positions around the breast. Results from previous studies [9] showed that circular array configuration is more suitable for clinical trials environment because it acquires many more reflection signals from the target object than planar array $((N - 1)^2 / 2VsN)$. It also provides much greater spatial diversity in the propagation paths of the reflected signals, allowing any dielectric scatter to be more precisely located [10].

To provide a quality microwave image, the existing antenna arrays require a large number of antennas which can be as large as several hundreds. The performance of an antenna array (for whatever application it is being used) increases with the number of antennas in the array. The drawback of course

Received 18 January 2015, Accepted 16 March 2015, Scheduled 5 April 2015

* Corresponding author: Lulu Wang (luwang@aut.ac.nz).

¹ AUT University, Institute of Biomedical Technologies, Auckland, New Zealand. ² Callaghan Innovation, Auckland, New Zealand.

is the increased cost, size and complexity. In general, the radiation pattern of an antenna array highly depends on the weighting method and the geometry of the array. However, the array configuration, especially in biomedical imaging applications, has received relatively little attention even though it strongly influences the radiation pattern.

This project investigates various two-dimensional (2-D) antenna array configurations to perform a high quality image with a fixed number of sensors. Several hundreds of antenna arrays have been designed, tested and analysed using our developed computer model. This paper presents the concept of using logarithmic spiral and random antenna arrays to generate high-resolution microwave images. Simulated and experimental investigations of logarithmic spiral and random antenna arrays by using our recently developed HMI technique [11–14] for imaging small inclusion embedded in a dielectric object are presented. The comparison of the proposed antenna arrays with the regularly spaced antenna array is also detailed. Whilst not fully representative of human tissue, the objects chosen for experimental study were deemed to be suitable for testing the validity of the antenna array configuration in the first instance.

2. ANTENNA AND ANTENNA ARRAY CONFIGURATIONS

2.1. Antenna Design

The flanged open-ended rectangular waveguide antenna (ORWA) is selected as transmitter and receivers due to the following benefits:

- It is compact enough to be located in a scanning arrangement.
- It is cost effective and widely available.
- The antenna is easy to move and be relocated on the array plane to study the performance of the antenna array.
- The small size also allows for the positioning of many antennas close to the imaging domain.

Figure 1(a) shows a schematic of the designed ORWA. The excitation port P is placed at 9 mm from the end of waveguide, and the dimensions are listed in Table 1. The WR62 waveguide that has a cut-off frequency of 9.5 GHz is used to design the ORWA shown in Figure 1(b). A small Male SMA connector is inserted through the sidewall of the waveguide. This enables the waveguide to be connected with an RG coaxial cable for measurement and analysis.

2.2. Antenna Array Configurations

Figure 2 displays the geometry relevant to the HMI imaging, where x , y and z represent antenna locations in the array plane. If a point $P(x, y, z)$ is assumed in the target dielectric object, under far-field conditions, the intensity distribution of the object $I(\underline{s})$ at position \underline{s} is defined as [13]:

$$I(\underline{s}) = \left(\frac{k_0^2}{4\pi}\right)^2 |\varepsilon(\underline{s}) - \varepsilon_1|^2 E_T(\underline{s}) \cdot E_T^*(\underline{s}') \quad (1)$$

Table 1. Dimensions of flanged ORWA.

Parameter	Dimension (mm)
Width of waveguide (A)	15.8
Length of waveguide (B)	7.9
Height of waveguide (H)	120
Thickness of the waveguide walls	1
Length of flange (L)	38
Width of flange (W)	2
Thickness of the flange (T)	6
Length of excitation port from the end of waveguide (P)	9

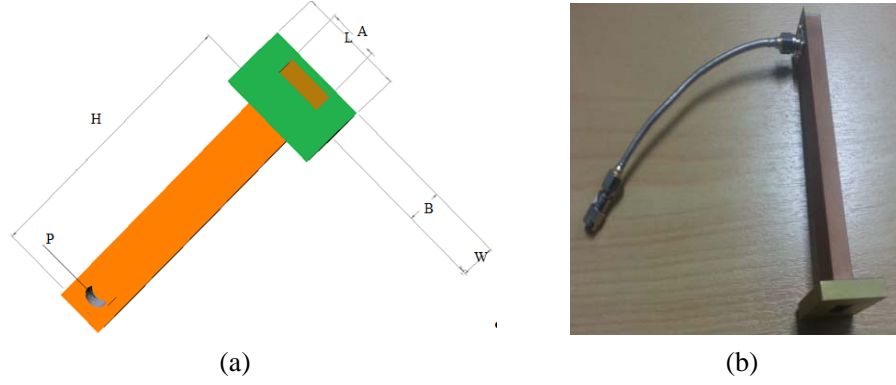


Figure 1. (a) Configuration of flanged ORWA. (b) Photograph of the flanged ORWA with connection cable.

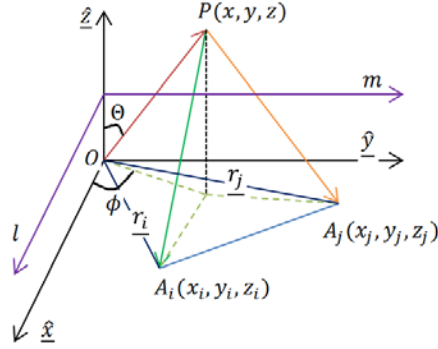


Figure 2. Geometry of HMI measurement by one pair of antennas.

k_0 = Free-space propagation;

$\varepsilon(\underline{s})$ = Complex relative permittivity distribution inside the dielectric object;

ε_1 = Relative permittivity of the host medium;

$E_T(\underline{s})$ = Total electric field (incident plus scattered) at a point inside the object with position vector, \underline{s} .

The back-scattered field quantity of a dielectric object, which we reconstructed at each voxel, is defined in (1), which we simply refer to as “intensity”. Physically, this quantity is proportional to the squared modulus of the polarisation charge density at each point inside the object. Note that this is a scalar quantity, which simplifies the image reconstruction.

In HMI system, all antennas are assumed to be located on a 2-D plane, then the 2-D image of projected scattering intensity within the dielectric object is reconstructed:

$$\tilde{I}(l, m) = \iint G(u, v) e^{j2\pi(ul+vm)} dudv \quad (2)$$

where (l, m) is defined as $(\sin \theta \cos \phi, \sin \theta \sin \phi)$ and refers to the polar coordinates as shown in Figure 2. $G(u, v)$ is the complex visibility data [13]. The complex visibility data can be computed by all possible pairs of receiving antennas, with the background scattered field subtracted from the data. For example, for N receivers, the measured complex visibility data are $N(N - 1)$.

The U - V coverage is developed for optimization of the antenna array configuration and object image. For any given pair of antennas $A_i(x_i, y_i, z_i)$ and $A_j(x_j, y_j, z_j)$, U - V coverage is defined as:

$$(u_{ij}, v_{ij}) = (x_j - x_i, y_j - y_i) / \lambda \quad (3)$$

where λ is the wavelength in free space.

Baseline B , equal to the difference between the antenna positions over the XY plane normalized

to the wavelength in free space, can be calculated by:

$$B_{ij} = \sqrt{(u_{ij})^2 + (v_{ij})^2} \quad (4)$$

Referring to Equation (2), a 2-D image of a dielectric object can be represented using complex visibility data collected when antenna array plane is placed at the selected height. The development of the 2-D HMI imaging algorithm is detailed in [12].

In order to design an antenna array plane more suitable for medical imaging applications using the HMI technique with lower cost and less operation time, the following factors need to be considered:

- The antenna array plane should contain as few antennas as possible.
- The antenna array should be able to provide dense sampling of the aperture (U - V coverage) over a wide range of projected baseline values.
- The antenna array should be able to offer the best possibility of detecting lesions anywhere within the target dielectric object.

A computer simulation model has been developed to investigate the antenna array configurations effect on image quality by using HMI applications. The authors have investigated hundreds of antenna arrays, and this paper only presents and compares selected spiral, random and regularly spaced arrays.

Antenna locations on a logarithmic spiral array flat plane (2-D) can be obtained by:

$$x = \frac{L(t \cos(t) + \min \|t \cos(t)\|)}{\max \|t \cos(t)\| + \min \|t \cos(t)\|} \quad (5)$$

$$y = \frac{W(t \sin(t) + \min \|t \sin(t)\|)}{\max \|t \sin(t)\| + \min \|t \sin(t)\|}$$

where $t = \text{linespace}(a\pi, \pi/b, N)$, a = Anticlockwise rotation angle, b = Clockwise rotation angle, N = Antenna number, L = Antenna array plane length, W = Antenna plane width.

Antenna locations on a random flat array plane can be calculated by using MATLAB random function:

$$(x, y) = \text{rand}(N, 2) \times L \quad (6)$$

where N = Antenna number, L = Antenna array plane length.

3. SIMULATION

3.1. Antenna Array Configurations

A mathematical computer simulation model was developed using MATLAB, and simulations using various antenna array configurations were performed to evaluate the proposed antenna arrays. This program quickly calculates and displays the U - V coverage of antenna arrays by combination of Equations (3), (5) and (6). All antennas are located on a flat plane (300 mm \times 300 mm). Three 16-element antenna array planes are shown in Figure 3, with one acting as a transmitting antenna and the remaining sensors acting as receiving antennas.

3.2. Target Dielectric Object

Figure 4 shows a 2-D view of the hemispherical shaped dielectric model (radius of 70 mm) with two spherical inclusions located at the same layer within the object. This dielectric object contains 2 mm thick dielectric material A ($\epsilon_r = 9.3$, $\sigma = 4\text{S/m}$), dielectric material B ($\epsilon_r = 9$, $\sigma = 0.4\text{S/m}$) and two lesions ($\epsilon_r = 9.5$, $\sigma = 7\text{S/m}$) of 5 mm in diameter. The space between the object and antenna array is assumed to be filled with air ($\epsilon_r = 1$, $\sigma = 0\text{S/m}$). The model was placed at $z = 0$ mm, and all antenna array planes were placed at $z = -450$ mm. Colour bar describes the complex relative permittivity of the dielectric object.

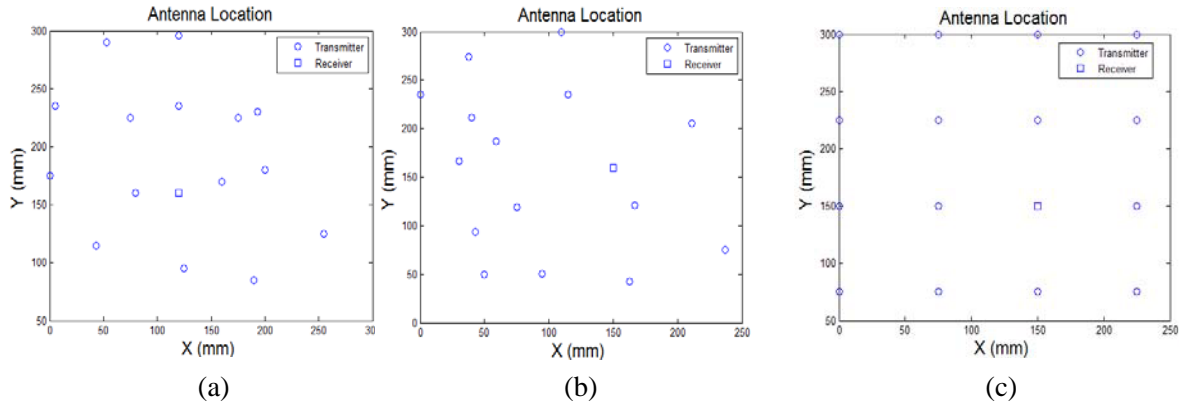


Figure 3. Antenna array configurations. (a) Spiral array. (b) Random array. (c) Regular spaced array.

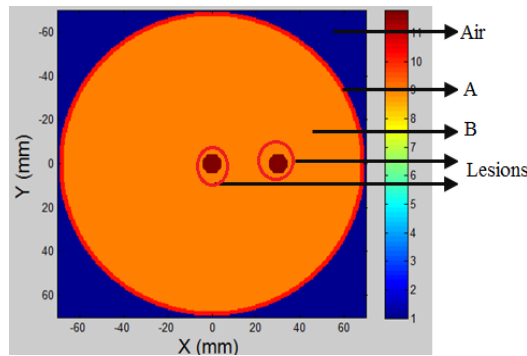


Figure 4. Original model under test.

3.3. Signal and Imaging Processing

During an operation, one port of a microwave generator excites a single transmitter at one frequency of 12.6 GHz [14]. The magnitude and phase of the backscattered electric field from the target object is measured at each receiver element in the array plane, which is connected to the second port of the microwave generator via a 16-channel switch. It will be shown in the following section that the complex valued data measured at each receiving antenna can be used to calculate the complex visibility data [13] for each possible pair of antennas. The complex visibility data then are used to form a 2-D image using an inverse Fourier transform. A computer with MATLAB software is used to analyse the reflected signals and generate images of the object under test by using the developed HMI imaging algorithms [11].

3.4. Simulation Results

Figure 5 displays the reconstructed 2-D images of dielectric object using the spiral, random and regularly spaced array configurations, respectively. Colour bars indicate the backscattered field from the model on a linear scale, normalised to the maximum in the 2-D images space. It can be seen that two lesions are fully reconstructed by using spiral and random arrays, but only artefacts are presented in the reconstructed image obtained by using regularly spaced array.

The simulation results of the same dielectric object that contains two lesions using a 16-element random antenna array configuration when the object was placed at a different height are detailed in [14]. Simulation results show that the best measurement distance range between the antenna array and the object is 450 mm to 550 mm. Measurement height out of the best range can cause artefacts, which make it difficult to identify lesions on the reconstructed images.

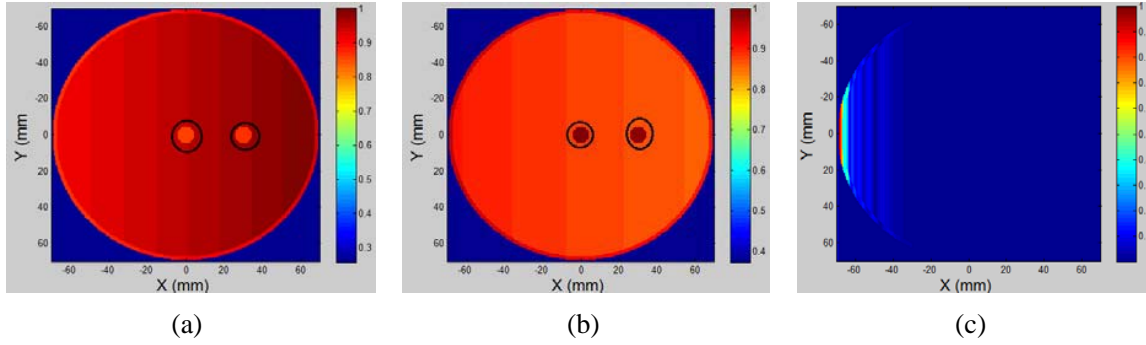


Figure 5. Reconstructed 2-D images using: (a) spiral antenna array, (b) random antenna array, (c) regularly spaced antenna array.

Table 2. Dielectric properties of materials at 12.6 GHz.

Material	Real part of permittivity	Imaginary part of permittivity	Size (mm)
External cube (100% wax)	2.43	0.24	100 by 100 by 30
Inclusion (Grape)	21.23	19.3	Diameters: 10

4. EXPERIMENTAL

4.1. Model and Materials

A dielectric object was used to test the proposed antenna array configurations that can be applied in holographic microwave imaging. The cube-shaped dielectric object consisted of an external cube made from an embedding medium and an inclusion. The external cube was made from emulsifying ointment that contained 30% emulsifying wax, 50% white soft paraffin and 20% liquid paraffin. Small grapes were inserted into the cube object to represent inclusion. The dielectric object was covered by a thin plastic film to minimize moisture loss and to make the object easier to handle. The plastic film has a negligible effect on the scattered electromagnetic field in the considered frequency range. Air ($\epsilon_r = 1$) was used as the medium filling the space between the dielectric object and antenna array.

4.2. Dielectric Properties Measurement

The actual dielectric properties of the external cube and inclusion were measured. Measurements with frequencies ranging from 10 GHz to 20 GHz were conducted using Agilent N5230A PNA and an Agilent 85070 single port dielectric probe. Reflection coefficients were converted to dielectric permittivity and loss tangent using Agilent 85070 dielectric measurement software.

A dielectric kit open-ended coaxial probe was connected to the network analyser for calibration. Probe calibration was carried out using three calibration standards: air, short-circuit and finally deionized water at a temperature of 21°C.

Following calibration, the probe was pressed against the sample ensuring no air gaps between the sample and probe. The reflection coefficient was measured and used to determine the permittivity. Data were recorded at 101 frequency points between 10 GHz and 20 GHz. This measurement was repeated three times in order to get an average reading. The sample must be thick enough to appear effectively semi-infinite to the probe. After measuring each object, the probe was cleaned with tissue paper to prevent any oil that may accumulate on it during measurements. The measured dielectric properties at 12.6 GHz ($\lambda = 23.8$ mm) of the external cube and inclusion are listed in Table 2.

4.3. Experimental System Setup

An experimental verification of the antenna arrays using the HMI technique was performed. Figure 6 shows an experimental setup of HMI data acquisition system which is detailed in [14]. An array

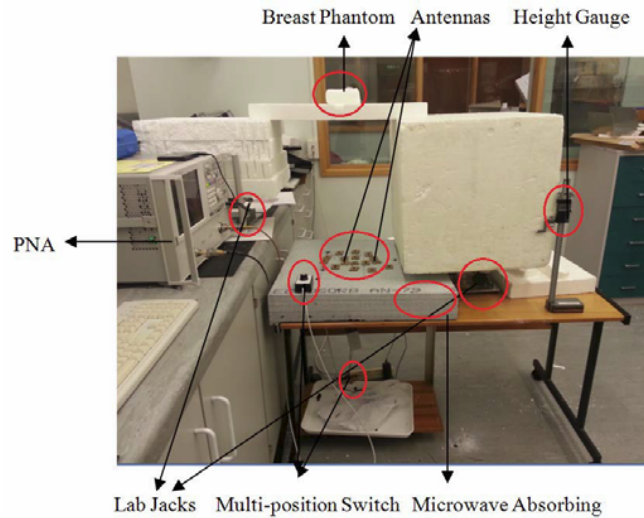


Figure 6. Photo of HMI system experimental set-up.

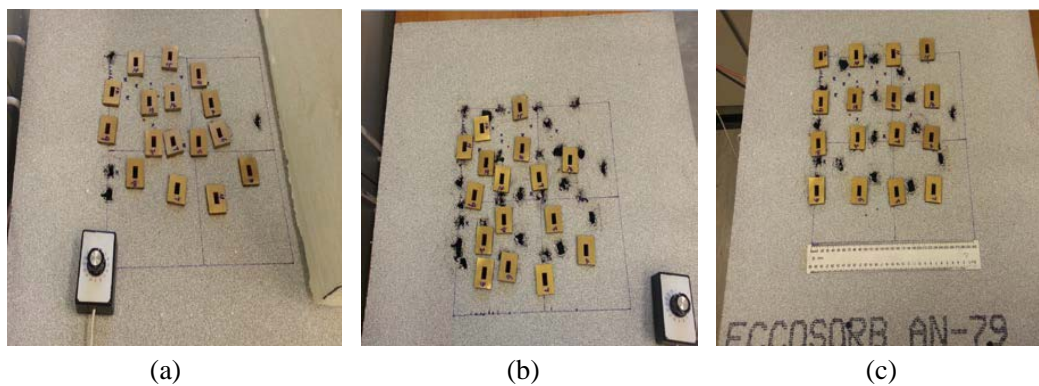


Figure 7. Experimental setup of antenna array planes: (a) spiral array, (b) random array, (c) regularly spaced.

of 16 antennas was embedded into a sheet of microwave absorbing material ECCOSORB AN-79 (600 mm \times 600 mm) and connected to an Agilent N5230A (10 MHz~20 GHz) PNA. Figure 7 displays the experimental setups of three antenna array configurations.

The dielectric object was illuminated using a transmitter, and the scattered field at each receiver was recorded at a frequency of 12.6 GHz [14]. The complex correlation of the scattered field data among all possible pairs of antennas was then computed to generate a complex visibility function that was used as the input to the HMI imaging algorithm.

4.4. Calibration

The measured signals include direct coupling between the antennas and reflections from the target object. Therefore, calibration is necessary to remove coupling noise. In this study, the calibration signal was the average of background measurements, i.e., with no test object present. This measured signal was subtracted from the actual response recorded for the target object at each receiving antenna. This step was repeated for every new vertical position of the antenna array. The antenna coupling signal was obtained both without the target object presence in the measurement (background) and with the image.

4.5. Data Acquisition

Although only a single frequency was used for reconstructing the image, the wide frequency spectrum from 10 GHz to 20 GHz was collected so that the optimal frequency could be determined. Data were recorded at 3201 frequency points for choosing the optimum frequency between 10 GHz and 20 GHz, and 101 measurements were averaged at each frequency. All 16 antennas were tested before data acquisition with one antenna as the transmitter and the 15 others as the receivers. Background data (i.e., with no object present) were collected at each receiver with the antenna array plane placed at $z = 540$ mm (22.7λ) before measuring the target object. This step was repeated three times and the data averaged. The dielectric object was illuminated by the transmitter and the backscattered field recorded at each receiver at the operating frequency of 12.6 GHz ($\lambda = 23.8$ mm) for all receivers located on the antenna array plane.

5. IMAGING RESULTS AND DISCUSSION

5.1. Reconstruction Results

Figure 8 shows the dielectric object (100 mm by 100 mm by 30 mm) including an external cube I and two inclusions of type I (10 mm in diameter), where the inclusions are located at $(X_1 = 50$ mm, $Y_1 = 50$ mm, $Z_1 = 20$ mm) and $(X_2 = 70$ mm, $Y_2 = 80$ mm, $Z_2 = 20$ mm). All antenna array planes are placed at $Z = -540$ mm

The 2-D reconstructed images (modulus part) of a dielectric object with different antenna array configurations are shown in Figure 9. Results indicate that two inclusions are detected clearly within

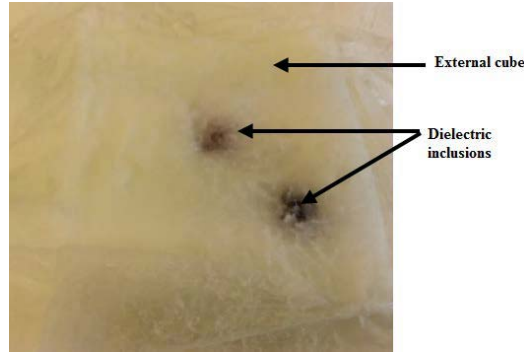


Figure 8. Photograph of the cube including two inclusions.

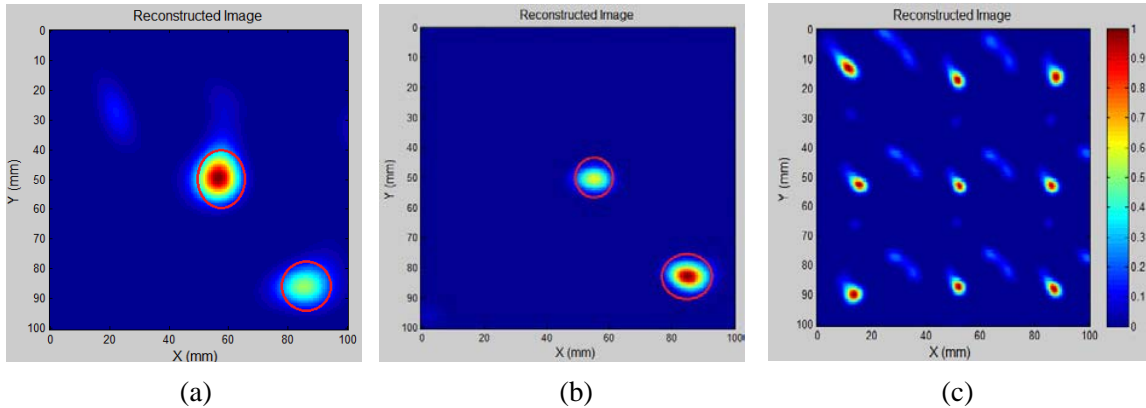


Figure 9. Reconstructed images of two inclusions using: (a) spiral antenna array, (b) random antenna array, (c) regularly spaced antenna array.

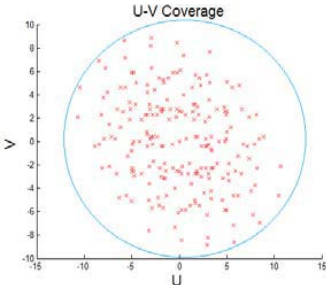
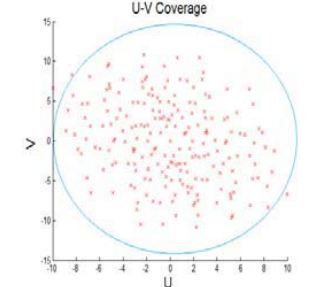
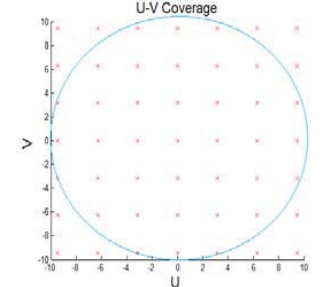
the reconstructed image when using spiral and random antenna arrays. As can be seen, the inclusions are not represented in the reconstruction image when using regularly spaced antenna array. Colour bars plot signal intensity on a linear scale that is normalised to the maximum in the 2-D image space. Values below 0.1 are rendered as blue.

5.2. Discussion

Table 3 compares the selected three samples of antenna array configurations. A quantitative analysis provides useful insight into the imaging performance of these arrays. $U-V$ density is defined as the maximum $U-V$ coverage value in the antenna array divided by the array plane size (mm^2). Results show that there is a significant difference of density, maximum, minimum, average and unique baseline among spiral, random and regularly spaced antenna arrays. $U-V$ coverages in Table 3 demonstrate that spiral and random arrays provide significantly denser sampling on the aperture plane over a wide range of the baseline than regularly spaced array. The image resolution is determined by density and unique baseline (different baseline) numbers in the antenna array, the sensitivity is determined by the minimum and average baseline in the antenna array.

Both simulated and experimental results show that lesions were successfully detected using the spiral and random array configurations but cannot be easily identified by visualization using the regularly spaced array configuration. It seems that image resolution is determined by the $U-V$ density and unique

Table 3. Comparison of various antenna array configurations.

Array	$U-V$ Coverage	Density	Minimum Baseline	Average Baseline	Unique Baseline Number
Spiral		0.1817	0.7846	3.1258	103
Random		0.1870	1.3188	3.4137	106
Regularly spaced		0.0176	3.1500	3.9387	10

baseline number in the antenna array plane. Higher value of U - V density with more unique baseline number produces a better quality microwave image.

The experimental results illustrate a good agreement with simulated ones. Results show that it is possible to produce a good quality dielectric object image using 16-element spiral and random arrays. Compared to the 31-element [15] and 64-element regular antenna arrays [16], the proposed spiral and random arrays have advantages in significantly reducing system cost and data acquisition time. Such antenna systems have many benefits, including low cost, short scanning time, steer ability, compactness, and simplicity of manufacturing process. Microwave imaging technique can be very helpful for medical imaging, food processing and agriculture applications [17] as well as security screening [18]. The potential applications of the proposed antenna array configurations using microwave imaging approach can be in the fields of medical imaging, security screening, food processing and agriculture.

The proposed antenna arrays provide the maximum combination of receiving antennas and enable the collection of out of plane transmission data. For a single transmitter and 15 receivers, the total number of 220 independent measurement points using the HMI technique is 210, but it is only 15 points for the same number of antennas using the microwave imaging approach detailed in [16]. This will significantly improve the image quality for a given number of antennas, whilst reducing the cost. A comparison of HMI results with other microwave imaging approaches will be investigated in the future.

The main drawback of the proposed arrays includes: all obtained images used HMI technique that was developed based on U - V coverage similar to the synthetic aperture radar technology in radio astronomy technology. Such antenna arrays may not be suitable for other microwave imaging approaches. Only a single transmitter is considered here in order to demonstrate the single-transmitter-multiple-receiver holographic microwave imaging system. The effect of multiple transmitters will be investigated in the near future.

6. CONCLUSION

This paper focuses on array configurations for a single-transmitter-multiple-receiver holographic microwave imaging system. Effort is made on simulations and measurement validation. Both simulated and experimental results demonstrate that using the same element antenna arrays, the spiral and random antenna arrays deliver clearer and more accurate images than the regularly spaced configuration. Random antenna array also provides the highest value of U - V density and offers the best possibility of detecting lesions within a dielectric object. The concepts of U - V density and baseline number are used to explain the image quality differences. In fact, each position in the U - V space represents a plane wave in a particular angular direction. The more angle it samples, the more detailed target features can be reconstructed.

Compared to the current widely used antenna array (regularly spaced array) in microwave imaging applications, the proposed antenna arrays have some advantages, including low cost, short scanning time, compactness, easy manufacture, and easy setup. Although the proposed array configurations were designed for HMI approach, they can also suit many other medical imaging applications, such as microwave imaging for brain stroke detection. Other potential applications of the proposed antenna arrays may include security screening and radio astronomical imaging, which will be investigated in the future.

REFERENCES

1. Ghavami, N., G. Tiberi, D. J. Edwards, and A. Monorchio, "UWB microwave imaging of objects with canonical shape," *IEEE Transactions on Antennas and Propagation*, Vol. 60, No. 1, 231–239, 2012.
2. Meaney, P. M., M. W. Fanning, T. Raynolds, C. J. Fox, Q. Fang, C. A. Kogel, and K. D. Paulsen, "Initial clinical experience with microwave breast imaging in women with normal mammography," *Academic Radiology*, Vol. 14, No. 2, 207–218, 2007.
3. Bond, E. J., X. Li, S. C. Hagness, and B. D. Van Veen, "Microwave imaging via space-time beamforming for early detection of breast cancer," *IEEE Transactions on Antennas and Propagation*, Vol. 51, No. 8, 1690–1705, 2003.

4. Fear, E. C., J. Bourqui, C. Curtis, D. Mew, B. Docktor, and C. Romano, "Microwave breast imaging with a monostatic radar-based system: A study of application to patients," *IEEE Trans. on Microwave Theory and Techniques*, Vol. 61, No. 5, 2119–2128, 2013.
5. Hagness, S. C., A. Taflove, and J. E. Bridges, "Two-dimensional FDTD analysis of a pulsed microwave confocal system for breast cancer detection: Fixed-focus and antenna-array sensors," *IEEE Transactions on Biomedical Engineering*, Vol. 45, No. 12, 1470–1479, 1998.
6. Li, X. and S. C. Hagness, "A confocal microwave imaging algorithm for breast cancer detection," *IEEE Microwave and Wireless Components Letters*, Vol. 11, No. 3, 130–132, 2001.
7. Fear, E. C., X. Li, S. C. Hagness, and M. A. Stuchly, "Confocal microwave imaging for breast cancer detection: Localization of tumors in three dimensions," *IEEE Transactions on Biomedical Engineering*, Vol. 49, No. 8, 812–822, 2002.
8. Rubæk, T., O. S. Kim, and P. Meincke, "Computational validation of a 3-D microwave imaging system for breast-cancer screening," *IEEE Transactions on Antennas and Propagation*, Vol. 57, No. 7, 2105–2115, 2009.
9. Semenov, S. Y., A. E. Bulyshev, A. Abubakar, V. G. Posukh, Y. E. Sizov, A. E. Souvorov, and T. C. Williams, "Microwave-tomographic imaging of the high dielectric-contrast objects using different image-reconstruction approaches," *IEEE Trans. on Microwave Theory and Techniques*, Vol 53, No. 7, 2284–2294, 2005.
10. O'Halloran, M., M. Glavin, and E. Jones, "Rotating antenna microwave imaging system for breast cancer detection," *Progress In Electromagnetics Research*, Vol. 107, 203–217, 2010.
11. Wang, L., A. M. Al-Jumaily, and R. Simpkin, "Holographic microwave imaging array for brain stroke detection," *Journal of Signal and Information Processing*, Vol. 4, No. 3B, 96–101, 2013.
12. Wang, L., R. Simpkin, and A. M. Al-Jumaily, "Holographic microwave imaging for medical applications," *Journal of Biomedical Science and Engineering*, Vol. 6, 823–833, 2013.
13. Wang, L., A. M. Al-Jumaily, and R. Simpkin, "Imaging of 3-D dielectric objects using far-field holographic microwave imaging technique," *Progress In Electromagnetics Research B*, Vol. 61, 135–147, 2014.
14. Wang, L., R. Simpkin, and A. M. Al-Jumaily, "Three-dimensional far-field holographic microwave imaging: An experimental investigation of dielectric object," *Progress In Electromagnetics Research B*, Vol. 61, 169–184, 2014.
15. Klemm, M., J. A. Leendertz, D. Gibbins, I. J. Craddock, A. Preece, and R. Benjamin, "Microwave radar-based differential breast cancer imaging: Imaging in homogeneous breast phantoms and low contrast scenarios," *IEEE Transactions on Antennas and Propagation*, Vol. 58, No. 7, 2337–2344, 2010.
16. Klemm, M., D. Gibbins, J. Leendertz, T. Horseman, A. W. Preece, R. Benjamin, and I. J. Craddock, "Development and testing of a 60-element UWB conformal array for breast cancer imaging," *Proc. 5th European Conf. Antennas and Propagation (EuCAP)*, 3077–3079, 2011.
17. Damez, J. L. and S. Clerjon, "Quantifying and predicting meat and meat products quality attributes using electromagnetic waves: An overview," *Meat Science*, Vol. 95, No. 4, 879–896, 2013.
18. Hu, T., Z. Xiao, J. Xu, and L. Wu, "Methods of personnel screening for concealed contraband detection by millimeter-wave radiometric imaging," *Procedia Engineering*, Vol. 7, 28–37, 2010.